Available online at www.sciencedirect.com
ScienceDirect
Journal of Molecular Structure 827 (2007) 176–187
Journal of MOLECULAR STRUCTURE
www.elsevier.com/locate/molstruc

Structure and vibrational assignment of 3,4-diacetyl-2,5-hexanedione. A density functional theoretical study

Sayyed Faramarz Tayyari [a,*], Mansoureh Zahedi-Tabrizi [b], Somayeh Laleh [a], Zainab Moosavi-Tekyeh [a], Hedayat Rahemi [d], Yan Alexander Wang [c]

[a] Department of Chemistry, Ferdowsi University, Mashhad 91774-1436, Iran
[b] Department of Chemistry, Alzahra University, Tehran 1993891167, Iran
[c] Department of Chemistry, Urmia University, Urmia 57159-165, Iran
[d] Department of Chemistry, University of British Colombia, Vancouver, Canada V6T 1Z1

Received 23 February 2006; received in revised form 14 May 2006; accepted 15 May 2006
Available online 10 July 2006

Abstract

Fourier transform infrared and Fourier transform Raman spectra of 3,4-diacetyl-2,5-hexanedione, known as tetraacetylethane (TAE) or α,α′-bis-acetylacetone, and its deuterated analogue have been obtained. Density functional theory (DFT) B3LYP and BLYP calculations have been carried out with the purpose of understanding the vibrational spectra of this compound and its deuterated analogue. The calculated geometrical parameters show a very strong hydrogen bond, compared with its parent molecule, acetylacetone (AA), with an O···O distance of 2.464–2.505 Å. This bond length is about 0.05–0.06 Å shorter than that for AA. According to the theoretical calculations, TAE has an asymmetric structure with a hydrogen bond strength of about 17.3 kcal/mol per bond (calculated with 6-311++G** basis set), about 1.4 kcal/mol more than that for AA. This increase in the hydrogen bond strength is consistent with the frequency shifts for OH/OD stretching, OH/OD out-of-plane bending, and O···O stretching modes and downfield proton chemical shift upon substitution of α-H atom with acetylacetone radical.

The geometries of keto–keto and some of the enol–keto tautomers were also fully optimized and compared with the enol–enol tautomer.

To investigate the effect of acetylacetone radical on the hydrogen bond strength, the charge distributions, steric effects, and Wiberg bond orders in TAE and AA were studied by the Natural Bond Orbital (NBO) method for optimized model compounds at B3LYP/6-31G** level of theory. The results of NBO analysis indicate that the steric effect is the main factor for increasing the hydrogen bond strength in TAE compared with that in AA.

Keywords: Vibrational spectra; 3,4-Diacetyl-2,5-hexanedione; Tetraacetylethane; Intramolecular hydrogen bond; NBO

1. Introduction

The *cis*-enol form of β-diketones is stabilized by a strong intramolecular hydrogen bond [1–4]. The vibrational spectra of these compounds have been the subject of numerous investigations, which support the existence of a strong intramolecular hydrogen bond of chelating nature in the enol form of β-diketones [5–13]. This hydrogen bond formation leads to the enhancement of the resonance conjugation of the π-electrons, which causes a marked tendency for equalization of the bond orders of the valence bonds in the resulting six-membered chelated ring. Therefore, it seems that any parameter that affects the electron density of the chelated ring will change the hydrogen bond strength. It is well known that substitution in α- or β-position drastically changes the hydrogen bond strength and the equilibrium between enol and keto tautomers [14–22]. In spite of several reports about the increasing hydrogen bond strength

* Corresponding author. Tel.: +98 511 8780216; fax: +98 511 8438032.
E-mail address: Tayyari@ferdowsi.um.ac.ir (S.F. Tayyari).

0022-2860/$ - see front matter © 2006 Elsevier B.V. All rights reserved.
doi:10.1016/j.molstruc.2006.05.028

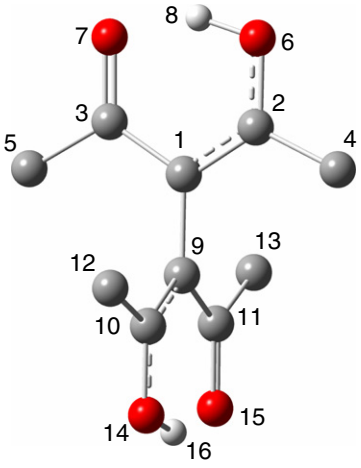

Fig. 1. Atom numbering system and structure of TAE (the H atoms of methyl groups are not shown).

upon substitution of α-position by electron withdrawing groups [14,15], Tayyari et al. [16] showed that charge removal from the enolated ring in fact reduces the hydrogen bond strength, while steric effect enhances the strength of the bond. It has also been shown that the hydrogen bond becomes stronger when bulky groups are involved [17–22]. The bulky groups have also pronounced effect on the keto–enol tautomerization. AA and α-methyl-AA exhibit 64% and 17% enol form in $CDCl_3$ solution, respectively [17].

TAE (Fig. 1) is of potential value as a monomer in the preparation of thermally stable polymers [23,24] and its use as a bifunctional chelating agent is obvious from its similarity to acetylacetone [25–27]. Tayyari et al. [5,6] showed that TAE predominantly exists as the *cis*-enol form and is engaged in a very strong intramolecular hydrogen bond, consistent with the X-ray and neutron diffraction results [28–30], which indicate a very short hydrogen bond of about 2.42–2.45 Å. Comparison of TAE and AA geometrical parameters gives a clear understanding of substitution effects of acetylacetone radical in α-position of AA on the structure and hydrogen bond strength of the system. This substitution is unique because it has no electron-withdrawing or -donating effect. Furthermore, since the two acetylacetone fragments are orthogonal, the direct resonance effect between the two AA radicals is also unlikely. Therefore we expect to study the pure steric effect of bulky substituents in α-position.

In this article, we will attempt to analyze the effect of the AA as a bulk substitute in the α-position and possible steric effects on the structure, hydrogen bond strength, and vibrational spectra of the enol form of β-diketones by means of DFT levels.

2. Experimental

TAE was prepared and purified according to the method described in the literature [31], mp 202 °C, ^{1}H NMR ($CDCl_3$): δ 2.01 (S, 12H, CH_3) and δ 16.81 (S, 2H, OH).

Partially deuterated TAE (D_2–TAE) was prepared by dissolving TAE in a boiling solution of acetone and D_2O, 5:1. The solution was allowed to cool down to room temperature; the crystals were separated and dried in vacuum. The method was repeated three times. Finally, D_2–TAE was recrystallized from a solution of acetone and D_2O.

The mid-IR spectra of D_2–TAE and its deuterated analogue were recorded by using Bomem MB-154 Fourier transform spectrophotometer in the region 500–4000 cm^{-1} in KBr pellet and in CCl_4 solution. The spectrum was collected with a resolution of 2 cm^{-1} by coadding the results of 15 scans.

The Raman spectra were collected employing a 180° back-scattering geometry and a Bomem MB-154 Fourier transform Raman spectrometer. The Raman spectrometer was equipped with a ZnSe beam splitter and a TE cooled InGaAs detector. Rayleigh filtration was afforded by two sets of two holographic technology filters. Laser power at the sample was 200 mw. The spectrum was collected with a resolution of 4 cm^{-1} by coadding the results of 200 scans.

The Far-IR spectra in the region 50–600 cm^{-1} were obtained using a Thermo Nicolet NEXUS 870 FT-IR spectrometer equipped with DTGS/polyethylene detector and a solid substrate beam splitter. The spectra were collected with a resolution of 4 cm^{-1} by coadding the results of 64 scans.

The NMR spectra were obtained on a FT-NMR, Brucker Aspect 3000 spectrometer at 100 MHZ frequency using 2 mol% solutions in $CDCl_3$ at 22 °C.

3. Method of analysis

The molecular equilibrium geometry and vibrational transitions of TAE were computed with the GAUSSIAN 03 [32] software system by using a selection of modern density functionals. The Becke's 1988, B, [33] and the Becke's three-parameters (B3) [34] exchange functionals with the correlation functional of Lee, Yang, and Parr, LYP [35,36] and the standard basis sets 6-31G*, 6-31G** and 6-311++G**.

To examine the presence of any keto form in the sample, the geometries of keto–keto, *cis*-keto, and *trans*-keto tautomers were also fully optimized at B3LYP/6-31G** level of theory. The results of these calculations were also compared with other conformers to examine the effects of conformation of one AA radical on the other.

The assignment of the experimental frequencies is based on the observed band frequencies and intensity changes in the infrared and Raman spectra of the deuterated species confirmed by establishing one to one correlation between observed and theoretically calculated frequencies.

Orbital population and Wiberg bond orders [37] were calculated with NBO 3.0 program implemented in Gaussian 03. Natural steric analysis [38,39] was performed at the B3LYP/6-311++G** level using NBO 5.0 program [40], which applied the wavefunction information file generated by the earlier version of NBO (3.0).

4. Results and discussions

4.1. Molecular geometry

The full-optimized structural parameters of *cis–cis* tautomer of TAE calculated at B3LYP level using 6-311++G**, 6-31G**, and 6-31G* basis sets and BLYP level using 6-31G** and 6-31G* basis sets with the corresponding experimental X-ray [29,30] results are summarized in Table 1. For comparison the optimized geometry of AA at the same levels of calculations and the results of its electron diffraction experiment [41] are also given in Table 1. The H-bond strength, E_{HB} (energy difference between the *cis*-enol and *trans*-enol conformers), OH stretching, OH out-of-plane bending, and proton chemical shift, of the enolated proton, for AA and TAE are compared in Table 2. To understand the effect of AA fragments on each other, the geometrical parameters of several keto, enol, and keto–enol tautomers of TAE, calculated at B3LYP/6-31G** level of theory, are listed in Table 3. The structures of these species are shown in Fig. 2.

Table 1 indicates that the calculated geometrical parameters are in good agreement with the observed results. The maximum deviation is observed for O···O distances, in which the calculated values are somewhat longer than the corresponding experimental distances and they are dependent on the basis set and level of calculation. This deviation is more pronounced with the 6-311++G** basis set. Nevertheless, these calculations clearly indicate that the O···O distance in TAE is about 0.05–0.06 Å shorter than that in AA, which is in excellent agreement with the observed value (0.06–0.07 Å). As Table 2 indicates, this shortening of O···O distance by substitution of H atom with the AA radical is consistent with the spectroscopic parameters, such as NMR chemical shift, OH stretching, and OH out-of-plane bending.

According to Table 1, B3 and B exchange functionals (with the same basis sets) give almost the same O···O distances, but the calculated O—H bond lengths obtained at

Table 1
Geometrical parameters and E_{HB} (kcal/mol) of TAE and AA[a]

	TAE							AA					
	A	B	C	D	E	X-ray[b]	X-ray[c]	A	B	C	D	E	E.D[d]
Bond lengths (Å)													
C1═C2	1.385	1.390	1.388	1.406	1.403	1.3908(7)	1.398(2)	1.370	1.374	1.372	1.389	1.367	1.382
C1—C3	1.459	1.457	1.461	1.461	1.466	1.4365(7)	1.426(2)	1.444	1.443	1.445	1.445	1.449	1.43
C2—O6	1.323	1.321	1.325	1.331	1.337	1.3090(6)	1.297(2)	1.326	1.325	1.328	1.336	1.34	1.319
O6—O7	2.485	2.464	2.501	2.465	2.505	2.4369(8)	2.449(2)	2.544	2.52	2.556	2.514	2.557	2.512
C3—O7	1.248	1.255	1.252	1.274	1.270	1.2700(6)	1.279(2)	1.246	1.252	1.25	1.272	1.269	1.243
O6—H8	1.010	1.022	1.014	1.052	1.039	0.997	1.148	1.003	1.013	1.009	1.041	1.033	1.049
C3—C5	1.512	1.514	1.516	1.524	1.527	1.4905(7)	1.495(2)	1.511	1.513	1.515	1.524	1.526	1.525
C2—C4	1.497	1.499	1.500	1.510	1.511	1.4915(8)	1.483(2)	1.494	1.497	1.498	1.507	1.508	1.493
C1—C9	1.495	1.494	1.496	1.503	1.504	1.4874(8)	1.488(2)	–	–	–	–	–	–
Bond angles (Å)													
C1C2O6	122.2	122.1	122.5	121.7	122.2	121.64(5)	122.23(14)	122.0	121.6	122.3	124.2	121.9	121
C2C1C3	118.1	117.4	118	117.3	117.9	117.71(4)	117.88(13)	120.8	120	120.6	119.8	120.5	119.7
C1C3O7	121.8	121.9	122.1	121.7	122.0	121.31(4)	121.15(14)	121.5	121.6	121.9	121.4	121.7	123
C5C3C1	119.9	120.1	119.8	120.6	125.2	120.78(4)	121.89(14)	118.9	118.9	118.6	119.6	119.2	118.1
C1C2C4	125.1	125.0	125.1	125.0	120.3	123.82(4)	123.15(15)	124.2	124.2	124.1	124.2	124.2	124.1
C2C1C9	121.6	121.9	121.6	121.9	120.6	121.64(4)	121.48(13)	–	–	–	–	–	–
C3C1C9	120.4	120.7	120.4	120.8	121.5	120.51(4)	120.63(13)	–	–	–	–	–	–
C4C2O6	112.7	113.0	112.4	113.3	112.7	114.54(4)	114.62(15)	113.8	114.0	113.6	114.4	113.9	114.9
C5C3O7	118.4	118.0	118.1	117.7	117.7	121.31(4)	116.95(14)	119.6	121.6	119.5	119.0	119.1	118.9
E_{HB}	34.5	37.5	36.7	37.9	37.1			15.9	17.4	17.2	17.8	17.6	

[a] A, B, and C are obtained at B3LYP using 6-311++G**, 6-31G**, 6-31G* basis sets, respectively, and D and E are obtained at BLYP level using 6-31G** and 6-31G* basis sets, respectively.
[b] Data from [30].
[c] Data from [29].
[d] Data from [39].

Table 2
Comparison between several properties involved in hydrogen bond strength in the enol form AA and TAE[a]

	E_{HB} (kcal/mol)	νOH (cm^{-1})	νOD (cm^{-1})	γOH (cm^{-1})	γOD (cm^{-1})	δ (ppm)
AA[b]	15.89	2850 in gas	2020	952	691	15.4
TAE	17.35	2580	1988	992	741	16.81

[a] E_{HB}, hydrogen bond energy (energy difference between I and III structures), calculated at the B3LYP/6-311++G**; ν, stretching frequency; δ, proton chemical shift; γ, out-of-plane bending frequency.
[b] Data from [10].

Table 3
Geometrical parameters of TAE tautomers calculated at B3LYP/6-31G** level of theory[a]

	cis–cis	*cis–trans*	tr–tr	ket–ket	*cis*–ket	tr–ket
Bond lengths (Å)						
C1—C2	1.3902	1.3887	1.3660	1.5447	1.3943	1.3732
O6—O7	2.464	2.4663	2.6303		2.4226	2.5497
C1—C3	1.4566	1.4566	1.4962	1.5513	1.4595	1.4988
C2—C4	1.4992	1.4993	1.5053	1.5151	1.5044	1.5085
C3—C5	1.5137	1.5137	1.5272	1.5113	1.5140	1.5286
C1—C9	1.4944	1.4991	1.5036	1.5629	1.5257	1.5384
C2—O6	1.3206	1.3219	1.3538	1.2167	1.3181	1.3500
C3—O7	1.2546	1.2548	1.2232	1.2163	1.2565	1.2234
C9—C10	1.3902	1.3666	1.3660	1.5425	1.5472	1.5370
C9—C11	1.4566	1.4969	1.4962	1.5594	1.5643	1.5454
C10—C12	1.4992	1.5054	1.5053	1.5211	1.5118	1.5194
C11—C13	1.5137	1.5273	1.5272	1.5131	1.5129	1.5096
C11—O15	1.2546	1.2229	1.2232	1.2155	1.2167	1.2190
C10—O14	1.3206	1.3528	1.3538	1.2167	1.2157	1.2162
Bond angles (°)						
C2C1C3	117.4	117.5	121.4	110.6	115.7	120.0
C10C9C11	117.4	121.3	121.4	110.3	99.4	113.2
C1C2C4	125.0	124.8	124.5	120.0	126.0	126.3
C1C3C5	120.1	120.0	117.2	118.9	123.4	120.4
C9C11C13	125.0	117.2	117.2	120.4	117.9	115.8
C9C10C12	120.1	124.7	124.5	119.9	115.4	119.9
C1C2O6	121.9	122.1	121.2	119.0	122.3	120.8
C1C3O7	122.1	121.9	123.3	118.6	120.7	121.9
C9C10O14	121.9	121.1	121.2	119.0	119.1	118.3
C9C11O15	122.1	123.3	123.3	118.3	121.7	122.3

[a] *cis*, *cis*-enol; tr, *trans*-enol; ket, keto.

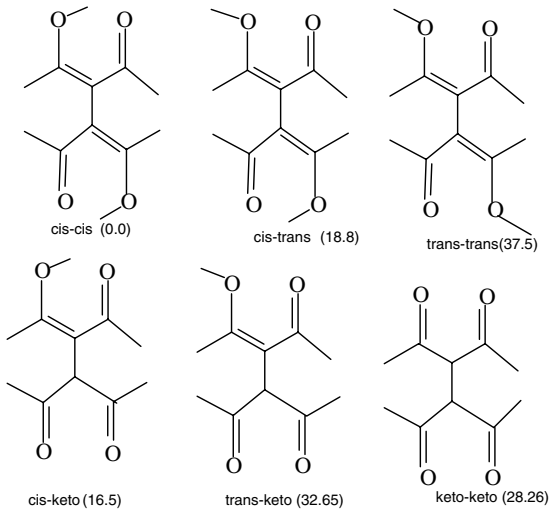

Fig. 2. The structure and relative energies (in kcal/mol) of the understudy tautomers of TAE.

these levels are different. These results lead to obtain a higher barrier height for proton transfer from one oxygen atom to another at the B3LYP level of calculation than that obtained with the BLYP level. Therefore, we expect to obtain weaker hydrogen bond (lower E_{HB}) with the B3LYP than that calculated at the BLYP level.

It is noteworthy that adding a polarized function on the hydrogen atoms causes considerable increase in the hydrogen bond strength (about 0.2 kcal/mol) and considerable decrease in the O···O distance (about 0.04 Å) of both AA and TAE molecules.

Table 1 also shows that upon AA substitution on α-position both C—C and C=C bond lengths are increased, whereas C—O and C=O bond lengths are decreased. These behaviors are explained in Section 4.2.2.

The reported crystallographic symmetry of TAE is 2(C2) but, in fact approximates closely to 42 m (D_2), consisting of two substantially planar halves twisted through almost 90° with respect to each other [28–30]. These results are consistent with our theoretical results.

As it is shown in Fig. 2, the hydrogen bond strength, the energy difference between *cis*- and *trans*-enol forms, 18.8 kcal/mol for the first AA fragment and 37.5 kcal/mol for both hydrogen bond system, is exactly twice of one single AA fragment. This result suggests that the two hydrogen bonded systems are almost independent of each other. The hydrogen bond strength per bond in TAE is about 1.0–1.4 kcal/mol stronger than that in AA. This calculated result is consistent with the other experimental observations given in Table 2.

The *cis–cis* tautomer is about 16.5 kcal/mol more stable than the *cis*-keto form (see Fig. 2). The keto–keto form is still more unstable than *cis*-keto form, about 11.8 kcal/mol. Therefore, the presence of any keto form in the sample is unlikely. The strength of hydrogen bond in *cis*-keto form, in spite of its very short O···O distance (2.424 Å), is less than 16.2 kcal/mol, which is considerably less than

that in *cis–cis* form per bond. This result could be explained by considering two factors: (1) the steric effect of keto form which pushes the O atoms together and (2) the electron-withdrawing effect of the diketo fragment in the *cis*-keto form, which decreases the strength of the bond.

Comparing the *cis–cis*, *cis–trans*, and *cis*-ket in Table 3 reveals that *trans* form of the substituted AA slightly weakens the intramolecular hydrogen bond in other part of molecule, whereas the keto form of substituted AA increases the strength of the bond. These results could be well explained by considering the steric effects, in the case of *cis–trans* the *trans* part of the molecule moves slightly away from the *cis* part and in *cis*-keto form the *cis* area is more crowded by the *trans* par of molecule. This change in the hydrogen bond strength, as could be observed from Table 3, also has considerable effects on the C—C, C=C, C—O, and C=O bond lengths of the *cis*-enol ring.

4.2. NBO analysis

4.2.1. Charge analysis

The charge distribution calculated by NBO method for optimized geometries of TAE and AA is tabulated in Table 4. According to this Table the most pronounced effect of substitution of α-H in AA by AA radical is reducing the charge over C_1. This is caused by electron-releasing nature of H, which disappears by AA radical substitution. Therefore, the AA radical compared with H acts as an electron-withdrawing group, which is expected to reduce the hydrogen bond strength. This effect is compensated by the steric effect of the AA radical which pushes the O atoms towards each other. The increase in the C=C and C—C bond lengths in TAE compared with those in AA could be explained by the charge redistribution. This effect causes to reduce the charge differences between C_1 with C_2 and C_1 with C_3 in TAE compared with those in AA. Therefore, we expect less coulombic attraction between $C_1^{\delta-}$–$C_2^{\delta+}$ and $C_1^{\delta-}$–$C_2^{\delta+}$, which leads to bond elongation.

4.2.2. Wiberg bond order

The calculated Wiberg bond orders for TAE and AA are compared in Table 5. This table shows that the C=C bond order in TAE is considerably reduced upon substitution of α-H by AA radical, about 0.05 Å. This Table also indicates that the C—C and C—O bond orders are reduced by this substitution but the C=O bond order does not show a pronounced change. These changes in the bond orders could be well explained if we consider the charge redistribution in the enol ring by replacement of H atom by AA radical. The H atom, as it was mentioned, acts as an electron supplying group, compared with the AA radical. Therefore, from charge transfer stand point, since the AA radical is not an electron-donating group, it is expected that replacing of H by AA radical reduces the electron density in the enol ring. This change in the charge density in the enol ring, as it was explained, results in lowering the bond orders compared with those in AA. This effect also tends to reduce the hydrogen bond strength [14]. On the other hand, the bulky AA radical pushes the O atoms towards each other and increases the hydrogen bond strength. The net result of these two opposite effects is reducing the O···O distance and, therefore, increases the hydrogen bond strength. Withdrawing electron from C=O group increases its bond order while increasing the hydrogen bond strength increases the π-electron conjugation which results in decreasing the bond orders of double bonds and increasing the bond orders of single bonds in the enol ring. These interpretations explain the resistance to change of the C=O bond order in TAE.

Table 4
Selected natural charge (e) distribution in TAE and AA

	TAE	AA
C1	−0.306	−0.494
C2	0.492	0.468
C3	0.550	0.535
O6	−0.682	−0.688
O7	−0.629	−0.629
H8	0.524	0.524

Table 5
Comparison of selected bond orders of TAE and AA

Bond	TAE	AA
C1=C2	1.4851	1.5459
C1—C3	1.1758	1.1987
C3=O7	1.5655	1.5783
C2—O6	1.2023	1.1788
O6—H8	0.5499	0.5714
O6···O7	0.0638	0.0593
O7···H8	0.1588	0.1373
C2—C4	1.0390	1.0404
C3—C5	1.0204	1.0171
C1—H9	–	0.9074
C1—C9	0.9941	–

4.2.3. Steric effect

The most important pairwise steric exchange energies, $\Delta E(i,j)$, interactions between NLMOs, which are absent in AA, are listed in Table 6. The sum of pairwise steric exchange $\Delta E(i,j)$ interactions in TAE (390 kcal/mol) is about 40 kcal/mol more than twice of those in AA (172 kcal/mol). This result confirms that steric effects play a determining role in shortening, thus strengthening the hydrogen bond, in TAE.

Table 6
Selected pairwise steric exchange energies ($\Delta E(i,j)$, kcal/mol, interactions between NLMOs *i*, *j* for TAE

NLMO (*i*)		NLMO (*j*)		$\Delta E_{i,j}$, kcal/mol
C1—C2	π	C9—C11	σ	4.89
C1—C2	π	C9—C10	σ	5.74
C1—C9	σ	C2—C4	σ	1.86
C1—C9	σ	C2—O6	σ	3.84
C1—C9	σ	C3—O7	σ	3.00
C1—C9	σ	C3—C5	σ	2.47
C4—H10	σ	C9—C11	π	3.00
C5—H22	σ	C9—C11	π	1.33

5. Vibrational analysis

Deconvoluted IR spectra of TAE and its deuterated analogue in the 850–1800 cm^{-1} are shown in Figs. 3 and 4, respectively. Lorentzian function has been utilized for deconvolution of the IR spectra. The Raman spectra of TAE and D_2–TAE in the solid phase are compared in Fig. 5.

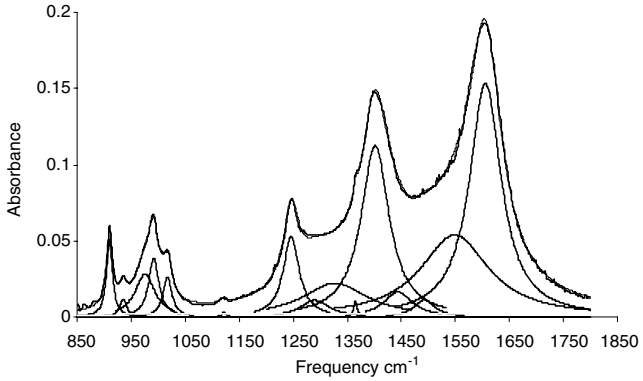

Fig. 3. The deconvoluted IR spectrum of TAE in CCl_4.

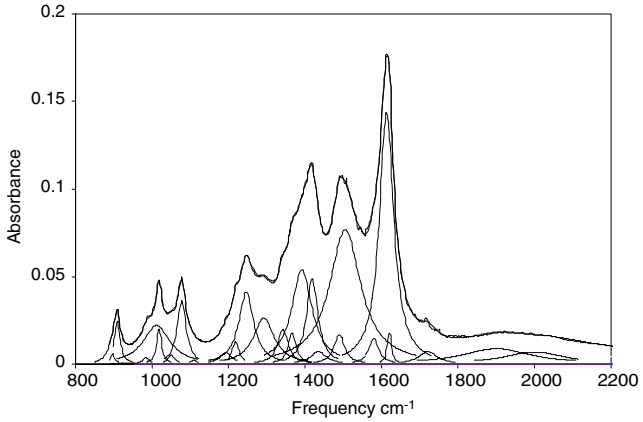

Fig. 4. The deconvoluted IR spectrum of D_2–TAE in CCl_4.

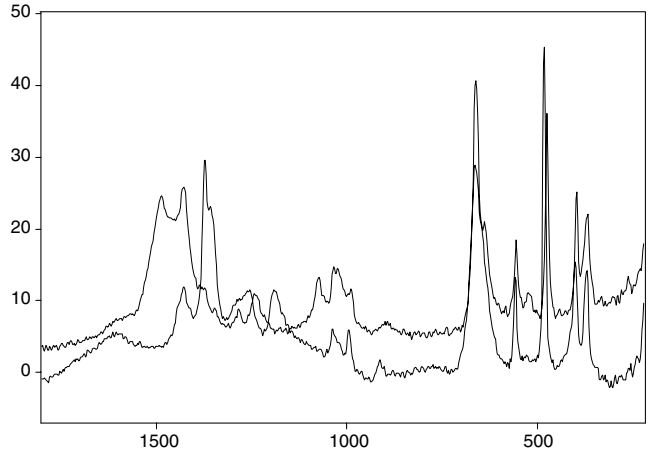

Fig. 5. Raman spectra of TAE (—) and D_2–TAE (···) in the solid state.

The observed and calculated (scaled) vibrational frequencies along with their approximate assignments for TAE and D_2–TAE are listed in Tables 7 and 8, respectively.

Ab initio harmonic vibrational frequencies are typically larger than the fundamental observed experimentally [42]. A major source of this disagreement is the neglect of the anharmonicity effects in the theoretical treatment. Measuring spectra in the condensed phases and incompleteness of basis sets in theoretical calculations are the other sources of discrepancies between observed and calculated frequencies. Zahedi-Tabrizi et al. [43] who recently studied the vibrational spectra of trifluoroacetylacetone showed that taking into account the anharmonicity in the calculations considerably improves the calculated results. Unfortunately, this kind of calculations is very time consuming and expensive. Nonetheless, it is found that the overestimation of *ab initio* harmonic vibrational frequencies is relatively uniform. Good overall agreement between the scaled theoretical harmonic frequencies and the anharmonic experimental frequencies has been reported [44].

Considering the infrared frequencies of MA and its deuterated analogues at below 2000 cm^{-1}, Larsen obtained excellent scaling factors for several DFT calculations [45]. Larsen's scaling factors are in good agreement with those obtained by Scott and Radom [44]. We found that there is no unique scaling factor for the whole range of the spectra. We obtained a scaling factor for the CH stretching region at each level of calculations, and then applied it to all frequencies above 1900 cm^{-1}, including the OH/OD stretching, which has been shown to be strongly anharmonic [43]. These scaling factors along with the corresponding regression coefficients and standard deviations are collected in Table 9. The residual errors of about 10 cm^{-1} are probable due to the deficiencies in the basis sets and higher order correlation effects not covered by B3LYP and BLYP levels and due to experimental errors. As shown in Tables 7 and 8, each observed band in the CH_3 stretching region consists of four normal modes, which could not be easily deconvoluted to their individual components. This problem is definitely a great source of errors in calculating more precise scaling factors. However, the results of our correlations are in close agreement with that obtained by Larssen and Cremer [46], who obtained a scaling factor of 0.957 with a regression coefficient of 0.985 for the CH stretching region by studying a large number of CH-containing systems. For all other frequencies below 1800 cm^{-1}, the scaling factors suggested by Larsen were applied [45].

The scaled theoretical vibrational frequencies calculated at several levels of theory along with the experimental results are given in Tables 7 and 8 for TAE and D_2–TAE, respectively. Tables 7 and 8 show an excellent agreement among the scaled frequencies at all levels of calculations and the experimental results for most of the frequencies. However, there are some relatively large disagreements between a few calculated frequencies obtained at different level of calculations. A close inspection of the Tables 7 and 8 tells us that these disagreements

Table 7
Calculated and observed vibrational spectra of TAE (frequencies are in cm^{-1})[a]

No.	Theoretical								Experimental					Assignment
	A	B	C	D	E	IR.I	R.A	dp	IR (CCl_4)	I	IR (solid)	R	I	
1	3031	3029	3032	3029	3030	2	42	0.74	3015	10	3007(w)	3006	5	νaCH_3
2	3030	3029	3032	3028	3030	10	11	0.74	3015	10	3007(w)	3006	5	νaCH_3
3	3016	3016	3017	3016	3017	9	51	0.37	3015	10	3007(w)	3006	5	νaCH_3
4	3016	3016	3017	3016	3017	17	100	0.75	3015	10	3007(w)	3006	5	νaCH_3
5	2966	2967	2970	2969	2970	5	22	0.73	2962	9	2971(w)	2970	15	νaCH_3
6	2966	2967	2969	2969	2970	7	59	0.66	2962	9	2971(w)	2970	15	νaCH_3
7	2960	2961	2964	2964	2964	4	173	0.75	2962	9	2971(w)	2970	15	νaCH_3
8	2959	2960	2963	2963	2963	5	10	0.75	2962	9	2971(w)	2970	15	νaCH_3
9	2916	2913	2915	2911	2918	2	137	0.04	2926	10	2927(w)	2926	100,p	νsCH_3
10	2915	2913	2915	2911	2917	1	206	0.03	2926	10	2927(w)	2926	100,p	νsCH_3
11	2915	2912	2914	2910	2917	10	299	0.06	2926	10	2927(w)	2926	100,p	νsCH_3
12	2915	2912	2914	2910	2916	11	213	0.08	2926	10	2927(w)	2926	100,p	νsCH_3
13	2530	2347	2776	2636	2809	371	27	0.06	2578	7	2570(w,br)	–		νOH
14	2528	2346	2775	2635	2808	413	18	0.42	2578	7	2570(w,br)	–		νOH
15	1587	1578	1625	1618	1623	75	7	0.24	1605	100	1600(vs)	1600	11,p	$\nu aC{=}C{-}C{=}O$
16	1584	1574	1624	1616	1617	534	3	0.75	1605	100	1600(vs)	1600	11,p	$\nu aC{=}C{-}C{=}O$
17	1616	1624	1606	1610	1598	211	57	0.04	1552	35	1550(s,br)	–		$\delta OH + \nu sC{=}C{-}C{=}O$
18	1609	1618	1595	1599	1593	346	9	0.75	1552	35	1550(s,br)	–		$\delta OH + \nu sC{=}C{-}C{=}O$
19	1468	1454	1457	1441	1452	2	4	0.59	1444	11	–	–		δaCH_3
20	1467	1453	1455	1440	1452	3	3	0.72	1444	11	–	–		δaCH_3
21	1466	1453	1455	1438	1447	22	11	0.70	1444	11	–	1440	sh	δaCH_3
22	1462	1448	1450	1434	1446	50	17	0.75	1444	11	–	1440	sh	δaCH_3
23	1461	1446	1450	1434	1445	21	20	0.34	1444	11	–	1440	sh	δaCH_3
24	1460	1446	1449	1433	1442	13	1	0.75	1444	11	–	–		δaCH_3
25	1447	1431	1435	1420	1432	0	9	0.71	–		–	1423	23	δaCH_3
26	1446	1430	1435	1418	1430	74	1	0.75	–		–	1423	23	δaCH_3
27	1392	1388	1399	1398	1397	28	8	0.61	1402	73	1406(vs)	–		$\delta sCH_3 + \nu aC{-}C{=}C{-}O$
28	1392	1387	1396	1395	1394	121	10	0.75	1402	73	1406(vs)	–		$\delta sCH_3 + \nu aC{-}C{=}C{-}O$
29	1379	1368	1377	1365	1376	59	10	0.11	1365	6	1367(w)	1372	61,p	$\nu C1{-}C9 + \delta OH + \delta sCH_3 + \nu C{=}C{-}C{=}O$
30	1373	1363	1372	1362	1372	2	43	0.00	1365	6	1367(w)	1372	61,p	$\nu C1{-}C9 + \delta OH + \delta sCH_3 + \nu C{=}C{-}C{=}O$
31	1356	1351	1370	1358	1369	48	4	0.69	1365	6	1367(w)	1372	61,p	$\delta sCH_3 + \delta OH + \nu aC{-}C{-}CH3$
32	1347	1348	1351	1344	1348	42	6	0.13	–		–	1358	sh	$\delta sCH_3 + \delta OH + \nu aC{-}C{=}C{-}O$
33	1343	1335	1346	1343	1348	70	4	0.24	–		–	1350	sh	$\delta sCH_3 + \delta OH + \nu aC{-}C{=}C{-}O$
34	1305	1272	1325	1307	1315	186	36	0.75	1328	14	–	–		$\nu aC{=}C{-}C + \delta OH + \nu C{=}C{-}C{=}O$
35	1265	1262	1273	1274	1268	202	14	0.75	1289	7	–	1296	sh	$\nu sC{-}C{=}C{-}O$
36	1229	1236	1230	1235	1237	169	1	0.75	1247	34	1254(s)	1253	21, p?	$\delta OH + \nu sC{=}C{-}C + \nu sC{-}CH_3$
37	1174	1170	1178	1176	1183	0	10	0.52	–		1190(sh)	1190	20, p	$\nu C1{-}C9 + \delta OH + \nu sC{-}CH_3$
38	1044	1032	1040	1030	1040	0	2	0.75	–		–	1038	8,dp?	ρCH_3
39	1039	1027	1036	1026	1036	0	0	0.75	–		–	1038	8,dp?	ρCH_3
40	1022	1016	1020	1016	1025	1	1	0.20	–		1031(sh)	–		ρCH_3
41	1022	1015	1020	1014	1024	3	1	0.75	–		1031(sh)	1027	sh,dp	ρCH_3
42	1015	1006	1013	1013	1017	9	1	0.59	1018	17	1018(s)	–		ρCH_3
43	1014	1004	1012	1012	1017	11	1	0.74	1018	17	–	–		ρCH_3
44	987	984	986	1005	992	41	1	0.74	992	25	997(s)	994	8	$\rho CH_3 + \nu C{-}CH3 + \nu C{-}C{-}O$
45	985	980	983	1003	988	51	4	0.22	992	25	997(s)	994	8	$\gamma OH + \rho CH_3$
46	981	1062	947	982	987	38	1	0.07	978	18,br	981(sh)	–		γOH
47	981	1061	947	978	986	64	0	0.74	978	18,br	981(sh)	–		γOH
48	921	925	922	925	931	22	1	0.75	936	8	936(m)	–		$\delta C{=}C{-}C$
49	892	893	896	895	903	19	2	0.21	910	32	910(s)	911	5,p	$\nu aC{-}CH_3 + \rho CH_3 + \Delta$ ring
50	891	891	894	894	901	30	1	0.75	910	32	910(s)	–		$\nu aC{-}CH_3 + \rho CH_3 + \Delta$ ring
51	655	656	659	659	676	5	1	0.39	673	4	678(w)	–		Γ
52	655	655	658	657	673	2	0	0.75	673	4	678(w)	–		Γ
53	642	642	644	642	650	8	22	0.02	–		–	662	56,p	Δ ring
54	626	625	628	626	635	10	5	0.75	635	2	640(vw)	650	sh	Δ ring
55	535	538	538	539	549	1	3	0.71	550*	sh	–	558	24	$\gamma C{-}CH_3$
56	533	535	535	536	548	0	0	0.74	550	sh	–	558	24	$\gamma C{-}CH_3$
57	514	517	512	513	521	6	3	0.07	536	s	541(w)*	–		$\Delta + \delta C{-}CH_3$
58	508	511	506	507	515	8	2	0.75	536	s	541(w)	–		$\Delta + \delta C{-}CH_3$
59	469	474	466	470	472	3	2	0.74	479	s	482(m)	483	91,p?	$\Delta + \delta C{-}CH_3$
60	469	473	465	469	472	4	2	0.75	479	s	482(m)	483	91,p?	$\Delta + \delta C{-}CH_3$
61	404	403	404	399	400	1	6	0.32	399	sh	–	401	27,dp	$\nu O\cdots O$
62	386	387	384	382	384	13	2	0.75	384	sh	397(mw)	–		$\nu sO\cdots O + \delta C{-}CH_3$
63	380	382	379	379	383	1	4	0.12	377	sh	375(m)	371	24,dp?	$\nu sO\cdots O + \delta C{-}CH_3$

Table 7 (*continued*)

No.	Theoretical								Experimental					Assignment
	A	B	C	D	E	IR.I	R.A	dp	IR (CCl_4)	I	IR (solid)	R	I	
64	354	352	354	353	363	3	2	0.75	371	m	375(m)	371	24,dp?	δC1—C9
65	354	352	354	352	359	2	2	0.67	371	m	375(m)	371	24,dp?	δC1—C9
66	270	272	269	268	270	3	0	0.75	n.m		290(w,br)	264	sh	Δ
67	194	197	193	193	194	1	1	0.26	n.m		212(w,br)	218	14	Δ
68	168	175	166	168	164	0	0	0.71	n.m		–	–		$\Gamma + \gamma C—CH_3$
69	167	174	163	168	163	0	0	0.75	n.m		–	–		$\Gamma + \gamma C—CH_3$
70	124	131	134	132	130	1	1	0.75	n.m		140(sh)	136	sh*	τCH_3
71	118	130	132	123	122	0	1	0.75	n.m		–	–		$\Gamma + \gamma aC—CH_3$
72	102	129	128	112	112	0	1	0.74	n.m		116(sh)	–		$\tau CH_3 + \gamma aC—CH3$
73	89	114	116	105	108	0	1	0.75	n.m		106(m)	106	sh	$\tau CH_3 + \gamma aC—CH3$
74	85	107	109	88	92	0	1	0.61	n.m		94(sh)	94	sh	Γ
75	80	101	101	87	81	2	1	0.75	n.m		–	–		$\tau CH_3 + \Delta ring$
76	78	82	79	80	79	3	2	0.75	n.m		–	–		γC1—C9
77	76	81	78	68	73	2	1	0.75	n.m		–	61	m	τCH_3
78	39	43	42	42	43	0	7	0.75	n.m		48(vw)	42	w	τC1—C9

[a] A, B, C, D, and E stands for scaled frequencies (cm^{-1}) calculated at BLYP/6-31G*, BLYP/6-31G**, B3LYP/6-31G*, B3LYP/6-31G**, and B3LYP/6-311++G**, respectively; IR, infrared; R, Raman; IR.I and R.A, and dp, IR intensity in KM/Mole, Raman scattering activities in Å**4/AMU, and depolarization ratio, respectively, calculated at B3LYP/6-311++G** level; I., relative intensity; v, very; s, strong; m, medium; w, weak; sh, shoulder; *, below 200 cm^{-1} are measured in different scale; *ν*, stretching; *δ*, in-plane bending; *γ*, out-of-plane bending; Δ, ring in-plane deformation; Γ, ring out-of-plane deformation; *ρ*, rocking; *τ*, torsion; n.m., not measured.

are limited to those frequencies related to the OH movements, such as νOH/νOD, δOH/δOD, and γOH/γOD. These behaviors are explainable if we recognize that these modes of vibration are highly dependent on the hydrogen bond strength. Since, as can be seen from Table 1 and discussed in Section 4.1, the calculated O···O distance, O—H bond length, and the hydrogen bond strength, E_{HB}, are very sensitive to the level of calculation and basis set used, we expect that those vibrational modes that are dependent on the hydrogen bond strength to be sensitive to the choice of basis set and level of calculation.

The vibrational frequencies calculated at B3LYP/6-311++G**, B3LYP/6-31G*, and BLYP/6-31G*, except for the CH and OH/OD stretching modes, are scaled by 0.9801, 0.9649, and 0.9976, respectively, according to the Spanget–Larsen results for malonaldehyde, the simplest β-diketone [43]. The applied scaling factors for the frequencies obtained at the B3LYP/6-31G** and BLYP/6-31G** levels are 0.9649 and 0.9976, respectively.

The scaled fundamental wavenumbers for TAE and D_2–TAE were compared with the experimental ones by means of two different regression analyses. In the first regression analysis, all available observed frequencies were selected. In the second regression analysis, the νOH/νOD, νC=C—C=O + δOH, and γOH/γOD normal modes were excluded from calculations. In these correlations, we used the available vibrational band frequencies in the CCl_4 solution and the available frequencies in the solid state Raman spectra if lacking the frequencies in solution. The results for these correlations are listed in Table 10 and clearly show that the calculated frequencies are generally in good agreement with the observed ones, but superior agreements can be obtained when the frequencies involved in the OH/OD motions are excluded from calculations. These results clearly indicate that the calculated frequencies at all considered levels are satisfactory, except for those involved in the OH/OD movements. Therefore, for these intramolecular hydrogen bonded systems, we should not expect to accurately obtain all vibrational frequencies simply by scaling calculated frequencies, since the strength of the bond is very sensitive to the choice of basis set and level of theory.

The assignment of the experimental frequencies is based on the observed band frequencies and intensity changes in the infrared and Raman spectra of the deuterated species confirmed by establishing one-to-one correlation between observed and theoretically calculated frequencies.

5.1. The OH/OD stretching mode

The IR spectrum of TAE in CCl_4 exhibits a very broad band in the 2000–3300 cm^{-1} regions, which upon deuteration of the enolic proton appears as a new band at about 2000 cm^{-1}. The IR spectrum of TAE in the CCl_4 solution exhibits a very broad band in the 1800–3300 cm^{-1} region centered at about 2580 cm^{-1}, which was assigned to OH stretching mode. As it is shown in Fig. 4, the deconvoluted D_2–TAE infrared spectrum exhibits two weak and relatively broad bands at about 2000 and 1900 cm^{-1} (on average 1950 cm^{-1}). These bands are likely to have occurred due to the proton tunneling phenomenon in the intramolecular symmetric hydrogen bonded system [47,48]. More study is necessary to insight this idea. The corresponding bands for AA and D_2-AA have been observed at about 2850 and 2020 cm^{-1}, respectively [10]. Lower band frequency of OH/OD stretching in TAE/D_2–TAE in comparison with those for AA/D_2-AA also supports the stronger hydrogen bond of TAE in comparison with that of AA [7].

Table 8
Calculated and observed vibrational spectra of D_2–TAE (frequencies are in cm^{-1})[a]

No.	Theoretical							Experimental			Assignment
	A	B	C	D	E	IR.I	R.A	IR (CCl_4)	IR (solid)[c]	R (solid)	
1	3031	3029	3032	3029	3030	2	54	3014(5)	3006,mw	3007,w	νaCH_3
2	3030	3029	3032	3028	3029	11	5	3014(5)	3006,mw	3007,w	νaCH_3
3	3016	3016	3017	3016	3017	7	60	3014(5)	3006,mw	3007,w	νaCH_3
4	3016	3016	3017	3016	3017	15	109	3014(5)	3006,mw	3007,w	νaCH_3
5	2966	2967	2970	2969	2970	5	54	2965(5)	2970,mw	2971,w	νaCH_3
6	2966	2967	2970	2969	2970	7	22	2965(5)	2970,mw	2971,w	νaCH_3
7	2960	2961	2964	2964	2964	4	175	2965(5)	2970,mw	2971,w	νaCH_3
8	2959	2960	2963	2963	2963	5	13	2965(5)	2970,mw	2971,w	νaCH_3
9	2916	2913	2915	2911	2918	2	198	2927(5)	2924,mw	2925,s	νsCH_3
10	2915	2913	2915	2911	2917	1	13	2927(5)	2925,mw	2925,s	νsCH_3
11	2915	2912	2914	2910	2917	7	375	2927(5)	2925,mw	2925,s	νsCH_3
12	2915	2912	2914	2910	2916	8	27	2927(5)	2925,mw	2925,s	νsCH_3
13	1866	1751	2035	1942	2059	256	7	1950(10,vbr)	~1900,br	–	νOD
14	1865	1750	2034	1941	2058	293	4	1950(10,vbr)	~1900,br	–	νOD
15	1585	1575	1624	1616	1621	39	1	1621(13)	1600,vs	1601,wbr	$\nu aC{=}C{-}C{=}O$
16	1582	1570	1620	1610	1615	540	4	1613(100)	1600,vs	1601,wbr	$\nu aC{=}C{-}C{=}O$
17	1489	1471	1505	1490	1501	156	46	1504(50)	1490,s	1483,s	$\nu sC{=}C{-}C{=}O + \delta OD$
18	1483	1465	1491	1477	1490	199	14	1504(15)	1490,s	1483,s	$\nu sC{=}C{-}C{=}O + \delta OD$
19	1468	1454	1456	1440	1452	3	8	–	–	1461,sh	δaCH_3
20	1467	1453	1455	1440	1451	2	12	–	–	1461,sh	δaCH_3
21	1466	1453	1455	1438	1447	19	34	–	–	1461,sh	δaCH_3
22	1460	1448	1449	1433	1442	10	1	1435(5)	–	–	δaCH_3
23	1448	1432	1439	1423	1435	37	40	1435(5)	–	1427,m	$\delta aCH_3 + \nu aC{-}C{=}C$
24	1446	1430	1435	1419	1431	101	32	1419(34)	1410,vs	1427,m	$\delta aCH_3 + \nu aC{-}C{=}C$
25	1430	1417	1431	1417	1427	77	29	1419(34)	1410,vs	1427,m	$\delta aCH_3 + \nu aC{-}C{=}C{-}O + \nu C{=}O$
26	1427	1415	1431	1416	1427	130	33	1419(34)	1410,vs	1427,m	$\delta aCH_3 + \nu aC{-}C{=}C{-}O + \nu C{=}O$
27	1390	1379	1399	1397	1397	23	11	1392(37)	1410,vs	–	$\delta C{-}CH_3 + \nu aC{-}C{=}C{-}O$
28	1388	1374	1394	1388	1388	42	0	1392(37)	–	–	$\nu sC{-}O + \nu sC{=}O + \nu C{-}CH_3$
29	1378	1368	1376	1363	1374	22	9	1366(12)	1360,sh,br	1371,m	$\delta sCH_3 + \nu C{-}C{=}C$
30	1372	1363	1370	1358	1369	35	15	1366(12)	1360,sh,br	1371,m	δsCH_3
31	1353	1350	1355	1346	1355	0	3	–	–	1346,vw	δsCH_3
32	1345	1344	1351	1344	1348	95	4	1342(9)	–	1346,vw	$\delta sCH_3 + \nu C{-}O$
33	1272	1284	1283	1291	1284	84	17	1291(18)	–	1281,w	$\nu sC{-}C{=}C{-}O + \delta OD$
34	1249	1244	1251	1250	1256	105	3	1246(29)	1240,s	1241,m	$\nu C1{-}C9 + \nu C{-}C + \delta OD$
35	1247	1243	1249	1249	1251	148	5	1246(29)	1240,s	1241,m	$\nu C{-}C + \nu C{-}CH_3$
36	1094	1092	1092	1094	1097	175	8	1078(25)	1070,ms	1072,m	$\delta OD + \nu C{=}C$
37	1040	1034	1041	1035	1042	0	5	–	–	1036,m	$\delta OD + \rho CH_3$
38	1044	1032	1038	1029	1038	1	1	–	–	1036,m	$\delta OD + \rho CH_3$
39	1039	1027	1036	1025	1035	2	1	–	–	1036,m	ρCH_3
40	1016	1012	1015	1008	1019	8	1	1018(15)	1018,s	1020,sh	ρCH_3
41	1016	1011	1014	1007	1019	9	2	1018(15)	1018,s	1020,sh	ρCH_3
42	1012	1006	1010	1003	1014	38	0	1012(15)	1010,sh	–	ρCH_3
43	1012	1004	1007	1003	1011	4	1	1012(15)	1010,sh	–	ρCH_3
44	979	976	975	972	980	15	4	984(3)	996,sh	989	ρCH_3
45	979	976	975	972	980	19	0	984(3)	996,sh	–	ρCH_3
46	907	908	908	909	918	2	1	909(17)	910,ms	912,w	$\delta OD + \nu aC{-}CH_3 + \nu C{-}C$
47	890	891	893	893	900	15	1	909(17)	910,ms	912,w	$\nu aC{-}CH_3$
48	885	887	884	887	889	21	0	897(5)	900,sh	–	$\nu aC{-}CH_3$
49	730	779	712	751	735	47	0	741[b]	742,s	–	γOD
50	729	779	711	750	734	44	0	741[b]	742,s	–	γOD
51	642	648	642	648	661	0	3	–	–	662,vs	Γ
52	640	646	636	644	658	1	0	660(4)	660,vw	–	Γ
53	637	637	636	637	646	12	15	–	–	640,m	Δ
54	620	618	622	620	629	13	5	628,sh	628(8)	–	Δ
55	534	537	536	538	548	2	4	–	–	552,m	Γ
56	532	534	534	535	547	1	0	549,vw	542,sh	–	Γ
57	511	515	509	511	518	7	4	525(6)	523(36)	526,w	Δ
58	502	505	500	502	509	7	2	525(6)	523(36)	526,w	Δ
59	466	471	462	466	468	2	2	475(10)	475(36)	475,s	Δ
60	465	471	461	466	468	4	2	475(10)	475(36)	475,s	Δ
61	386	384	387	383	387	0	5	n.m	397,vw	397,m	$\nu O{-}O + \delta C{-}CH_3 + nA\text{-}A$
62	378	378	378	374	377	13	5	n.m	372,m	372,m	$\nu O{-}O + \delta C{-}CH_3$
63	378	377	377	374	376	3	2	n.m	372,m	372,m	$\nu O{-}O + \delta C{-}CH_3$

Table 8 (*continued*)

No.	Theoretical							Experimental			Assignment
	A	B	C	D	E	IR.I	R.A	IR (CCl_4)	IR (solid)[c]	R (solid)	
64	354	352	354	352	362	5	2	n.m	372,m	369,sh	δAc—Ac
65	353	352	352	351	358	2	2	n.m	372,m	369,sh	δAc—Ac
66	267	268	266	264	265	3	0	n.m	–	263,vw	νO—O + δC—CH_3
67	194	196	193	193	194	1	1	n.m	210,vw	210,w	
68	168	175	165	168	163	0	0	n.m	–	–	Γ
69	166	174	163	167	162	0	0	n.m	–	–	Γ
70	124	131	134	132	130	1	1	n.m	140,w	132,sh*	γC—CH_3 + τCH_3
71	118	130	132	122	122	0	1	n.m	–	–	γC—CH_3 + τCH_3
72	102	129	128	112	112	0	0	n.m	112,sh	–	Γ + γC—CH_3
73	89	114	116	105	108	0	0	n.m	102,m	104,sh*	Γ + γC—CH_3
74	85	107	109	88	92	0	0	n.m	94,sh	92,s*	τCH_3
75	80	101	100	86	80	2	1	n.m	–	–	τCH_3 + γAc—Ac
76	77	81	79	79	78	3	2	n.m	–	78,sh*	τCH_3
77	76	80	77	68	73	2	1	n.m	–	62,w*	τCH_3
78	39	43	42	42	43	0	6	n.m	45,vw	42,s*	τ—Ac—Ac

[a] See footnotes of Table 7.
[b] Measured in CS_2.
[c] Data from Refs. [5,31].

Table 9
Scaling factor α, regression coefficient *R*, and standard deviation SD for regression of observed CH stretching wavenumbers on theoretical ones (see text)

	α	*R*	SD (cm^{-1})
B3LYP/6-311++G**	0.960	0.9723	9
B3LYP/61G**	0.952	0.9551	11
B3LYP/6-31G*	0.952	0.9616	10
BLYP/6-31G**	0.977	0.9630	10
BLYP/6-31G*	0.978	0.9683	10

Table 10
Scaling factor α, regression coefficient R, and standard deviation SD for regression of observed vibrational wavenumbers on theoretical ones (see text)[a]

	Method I[b]			Method II[c]		
	α	*R*	SD (cm^{-1})	α	*R*	SD (cm^{-1})
TAE						
A	1.001	0.99977	19	1.001	0.99987	15
B	1.007	0.99884	44	1.003	0.99987	14
C	0.994	0.99924	35	1.000	0.99991	12
D	0.999	0.99979	19	1.003	0.99992	11
E	0.992	0.99910	38	1.000	0.99995	9
D_2–TAE						
A	1.003	0.99979	18	1.001	0.99903	13
B	1.007	0.99924	35	1.003	0.99980	13
C	0.998	0.99979	18	1.000	0.99993	11
D	1.002	0.99993	10	1.003	0.99994	10
E	0.997	0.99977	19	1.000	0.99997	8

[a] A, B, C, D, and E stands for the BLYP/6-31G*, BLYP/6-31G**, B3LYP/6-31G*, B3LYP/6-31G**, and B3LYP/6-311++G** levels of theory, respectively.
[b] All observed frequencies were considered.
[c] For TAE, the frequency numbers 13, 14, 17, 18, 46, and 47 and for D_2–TAE, the frequency numbers 13, 14, 36–38, 49, and 50 were excluded from regression calculations.

5.2. The 1000–1700 cm^{-1} region

Besides the CH_3 deformation modes, five pairs (due to the symmetric and asymmetric vibrations) of bands related to the enol ring modes are expected to be observed in this region, which are attributed to the combinations of the C=O, C—O, C=C, C—C stretching and the OH bending modes [10–13]. The type of combinations depends on the extent of π-delocalization and bond equalizations in the enol ring. Deconvoluted IR spectrum of TAE in CCl_4 solution indicates that in the C=O and C=C stretching region two bands exist at 1605 and 1552 cm^{-1}, and upon deuteration the latter appears at 1505 cm^{-1}. The corresponding bands for AA were observed at 1625 and 1600 cm^{-1}, respectively [10]. The former, a very strong band and almost insensitive to the deuteration, is assigned to the asymmetric C=C—C=O stretching and the latter, a broad band, is assigned to the symmetric C=C—C=O stretching strongly coupled with the OH in-plane bending mode.

As shown in Table 7, the corresponding calculated scaled frequencies (at B3LYP/6-311++G**) are obtained, on average, at 1620 and 1595 cm^{-1}, respectively. This frequency difference could be attributed to the difference in media for obtaining the calculated and experimental results and the existence of the strong anharmonicity in the potential surface of this kind of hydrogen bonded system [43]. However, the most important source for these discrepancies is the error in estimation of the hydrogen bond strength, which is very sensitive to the choice of basis set and level of calculation. The theoretical position of these two bands calculated at the BLYP is reversed, which could be explained by considering the overestimation of hydrogen bond strength (see Table 1). Considerably large difference between 1552 cm^{-1} band and its corresponding theoretical band at 1595 cm^{-1} (calculated at the B3LYP/

6-311++G**) is mainly due to the participation of OH bending in this mode of vibration. Coincidence of the corresponding theoretical and experimental frequencies at about 1500 cm^{-1} in the deuterated analogue, which is decoupled from the OD bending, confirms this explanation. The same situation has been also reported before for α-cyano-acetylacetone [49], which also exhibits a strong intramolecular hydrogen bond.

Upon deuteration the Raman band at 1253 cm^{-1} disappears and two new Raman bands appear at 1072 and 1036 cm^{-1}, where the former is relatively strong and the latter is inactive in the IR spectrum. These observations are nicely in agreement with the calculation results. According to the calculations, the 1253 cm^{-1} band is mainly caused by the OH in-plane bending strongly coupled to the symmetric C—C=C stretching motion. The corresponding bands in the deuterated analogue, 1072 and 1036 cm^{-1}, are caused by OD in-plane bending, coupled to the C=C stretching and CH_3 rocking modes, respectively. Raman activity of these bands supports the assignments.

According to the calculations the observed Raman band at 1190 cm^{-1} is assigned to the C_1—C_9 stretching strongly coupled to the OH stretching. Upon deuteration, this band shifts to 1246 cm^{-1}.

5.3. Below 1000 cm^{-1}

In this region one expects to observe C=CH_3 stretching, OH and C=H out-of-plane bending, CH_3 deformation modes and the in-plane and out-of-plane ring deformations. The medium and relatively broad IR band at 978 cm^{-1} is assigned to γOH, which upon deuteration shifts to 741 cm^{-1}.

The IR band at 936 cm^{-1} is absent in the Raman spectrum. We correlated this band to the theoretical band at 931 cm^{-1} on the basis of calculated Raman and IR intensities. This band corresponds to the in-plane C=C—C bending mode.

By considering the theoretical calculations, the medium IR band at 910 cm^{-1} in TAE is assigned to νaC=CH_3 and ρCH_3, which causes a kind of deformation in the enol ring. The corresponding band in AA, which occurs at 915 cm^{-1}, upon deuteration shifts upward about 20 cm^{-1} [10] but in TAE this shift is negligible. The higher frequency shift of this band in AA upon deuteration could be attributed to its coupling with the C–D in-plane bending mode in deuterated AA.

The strong bands at 673 cm^{-1} and 662 cm^{-1} in the IR and Raman spectra, respectively, are attributed to the out-of-plane ring deformation modes that are considerably higher than the corresponding mode in AA. This could be attributed to firmer enol ring of TAE in comparison with that in AA. This is caused by stronger intramolecular hydrogen bond in TAE than that in AA.

An important band frequency in this region is the O···O stretching which is occurring at about 400 cm^{-1}, considerably higher than that in AA, 366 cm^{-1} [10]. This result is also in line with the stronger intramolecular hydrogen bond in TAE compared with that in its parent, AA.

6. Conclusion

The full optimized geometries of the *cis*-enol forms and the corresponding *trans*-enol forms of TAE and AA are fully optimized at the B3LYP level of theory using 6-31G*, 6-31G**, and 6-311++G** basis sets and at the BLYP level using 6-31G* and 6-31G** basis sets. The results of DFT calculations indicate that the calculated hydrogen bond strength, the O···O distance, and O—H bond length are very sensitive to the choice of level of calculation and basis set. However, the results of all calculations indicate that the intramolecular hydrogen bond in TAE is considerably stronger than that in its parent, AA. According to the NBO calculations, this increase in the hydrogen bond strength is solely caused by the steric effects.

The results of calculations on the keto and *trans*-enol conformers exclude the presence of these conformers in the sample, which is in agreement with the experimental results.

The vibrational frequencies of TAE and D_2–TAE were calculated at all aforementioned levels of theory. The predicted scaled frequencies, IR and Raman intensities, and depolarization ratios were compared with the corresponding experimental results. Although, a discrepancy was observed for a few wavenumbers due to the strong anharmonicity in the proton potential movement, in general a satisfactory reproduction of the experimental data is obtained.

Acknowledgements

We are grateful to the University of Ferdowsi (Mashhad) for its support of this research. Y.A.W. gratefully acknowledges the financial support from the Natural Sciences and Engineering Research Council (NSERC) of Canada. WestGrid and C-HORSE have partially provided the necessary computational resources.

References

[1] A.H. Lowery, C. George, P.D. Antonio, J. Karle, J. Am. Chem. Soc. 93 (1971) 6399.
[2] R.S. Brown, A.T. Nakashima, R.C. Haddon, J. Am. Chem. Soc. 101 (1979) 3175.
[3] J. Emsley, Struct. Bond 57 (1984) 147.
[4] R. Boese, M.Y. Antipin, D. Blaser, K.A. Lyssenko, D. Blăser, K.A. Lyssenko, J. Phys. Chem. B 102 (1998) 8654.
[5] S.F. Tayyari, T. Zeegers-Huyskens, J.L. Wood, Spectrochim. Acta A 35 (1979) 1265.
[6] S.F. Tayyari, T. Zeegers-Huyskens, J.L. Wood, Spectrochim. Acta. A 35 (1979) 1289.
[7] T. Chiavassa, P. Verlaque, L. Pizalla, P. Roubin, Spectrochim. Acta A 50 (1993) 343.
[8] T. Chiavassa, P. Roubin, L. Pizalla, P. Verlaque, A. Allouche, F. Marinelli, J. Phys. Chem. 96 (1992) 659.

[9] E. Bosch, M. Moreno, J.M. Liuch, J. Am. Chem. Soc. 114 (1992) 2072.
[10] S.F. Tayyari, F. Milani-Nejad, Spectrochim. Acta A 56 (2000) 2679.
[11] S.F. Tayyari, F. Milani-Nejad, Spectrochim. Acta A 54 (1998) 255–263.
[12] S.F. Tayyari, F. Milani-Nejad, H. Rahemi, Spectrochim. Acta A 58 (2002) 1679.
[13] S.F. Tayyari, S. Salemi, M. Zahedi-Tabrizi, M. Behforouz, J. Mol. Struct. 694 (2004) 91.
[14] Z. Yoshida, H. Ogoshi, T. Tokomitsu, Tetrahedron 26 (1970) 5691.
[15] G. Buemi, F. Zuccarello, Electr. J. Theor. Chem. 2 (1997) 302.
[16] S.F. Tayyari, Z. Moosavi-Tekyeh, M. Zahedi-Tabrizi, E. Eshghi, J.S. Emampour, H. Rahemi, M. Hassanpour, J. Mol. Struct. 782 (2006) 191.
[17] L.W. Reevs, Can. J. Chem. 35 (1957) 1351.
[18] J. Emsely, L.Y.Y. Ma, S.C. Nyburg, A.W. Parkins, J. Mol. Struct. 240 (1990) 59.
[19] J. Emsely, L.Y.Y. Ma, Bates, M. Motevalli, M.B. Hursthouse, J. Chem. Soc. [Perkin I] 2 (1989) 527.
[20] J. Emsely, L.Y.Y. Ma, S.A. Karaulov, M. Motevalli, M.B. Hursthouse, J. Mol. Struct. 216 (1990) 143.
[21] J. Emsely, N.J. Freeman, P.A. Bates, M.B. Hursthouse, J. Chem. Soc. [Perkin I] (1988) 297.
[22] G. Buemi, F. Zuccarello, Electr. J. Theor. Chem. 2 (1997) 302.
[23] Y. Zhang, S. Wang, G.D. Enright, S.R. Breeze, J. Am. Chem. Soc. 120 (1998) 9398.
[24] Y. Zhang, S.R. Breeze, S. Wang, J.E. Greedan, N.R. Raju, L. Li, Can. J. Chem. 77 (1999) 1424.
[25] S. Yamazaki, Polyhedron 11 (1992) 1983.
[26] S.K. Berzhanova, D.K. saltybayev, B.A. Zhuanov, Ye.V. Gutsalyuk, Polym. Sci. USSR 25 (1983) 2512.
[27] T. Sakai, Z. Taira, S. Yamazaki, Polyhedron 12 (1993) 2133.
[28] J.P. Schaefer, P.J. Wheatley, J. Chem. Soc. (A) (1966) 528.
[29] L.F. Power, K.E. Turner, F.H. Moore, J. Chem. Cryst. 5 (1975) 59.
[30] K.A. Lyssenko, D.V. Lyubetsky, M.Yu. Antipin, Mendeleev Comm. 13 (2003) 60.
[31] S. F. Tayyari Thesis, London University, 1978.
[32] Gaussian 03, Revision B.05, M.J. Frisch, G.W. Trucks, H.B. Schlegel, G.E. Scuseria, M.A. Robb, J.R. Cheeseman, J.A. Montgomery, Jr., T. Vreven, K.N. Kudin, J.C. Burant, J.M. Millam, S.S. Iyengar, J. Tomasi, V. Barone, B. Mennucci, M. Cossi, G. Scalmani, N. Rega, G.A. Petersson, H. Nakatsuji, M. Hada, M. Ehara, K. Toyota, R. Fukuda, J. Hasegawa, M. Ishida, T. Nakajima, Y. Honda, O. Kitao, H. Nakai, M. Klene, X. Li, J.E. Knox, H.P. Hratchian, J.B. Cross, C. Adamo, J. Jaramillo, R. Gomperts, R.E. Stratmann, O. Yazyev, A.J. Austin, R. Cammi, C. Pomelli, J.W. Ochterski, P.Y. Ayala, K. Morokuma, G.A. Voth, P. Salvador, J.J. Dannenberg, V.G. Zakrzewski, S. Dapprich, A.D. Daniels, M.C. Strain, O. Farkas, D.K. Malick, A.D. Rabuck, K. Raghavachari, J.B. Foresman, J.V. Ortiz, Q. Cui, A.G. Baboul, S. Clifford, J. Cioslowski, B.B. Stefanov, G. Liu, A. Liashenko, P. Piskorz, I. Komaromi, R.L. Martin, D.J. Fox, T. Keith, M.A. Al-Laham, C.Y. Peng, A. Nanayakkara, M. Challacombe, P.M.W. Gill, B. Johnson, W. Chen, M.W. Wong, C. Gonzalez, J.A. Pople, Gaussian, Inc., Pittsburgh PA, 2003.
[33] A.D. Becke, Phys. Rev. A 38 (1988) 3098.
[34] A.D. Becke, J. Chem. Phys. 98 (1993) 5648.
[35] B. Miehlich, A. Savin, H. Stoll, H. Preuss, Chem. Phys. Lett. 157 (1989) 200.
[36] C. Lee, W. Yang, R.G. Parr, Phys. Rev. B 37 (1988) 785.
[37] K.W. Wiberg, Tetrahedron 24 (1968) 1083.
[38] J.K. Badenhoop, F. Weinhold, J. Chem. Phys. 107 (1997) 5406.
[39] A.E. Reed, L.A. Curtiss, F. Weinhold, Chem. Rev. 88 (1988) 899.
[40] NBO 5.0. E.D. Glendening, J.K. Badenhoop, A.E. Reed, J.E. Carpenter, J.A. Bohmann, C.M. Morales, F. Weinhold (Theoretical Chemistry Institute, University of Wisconsin, Madison, WI, 2001); http://www.chem.wisc.edu/~nbo5.
[41] K. Iijima, A. Ohnogi, S. Shibata, J. Mol. Struct. 156 (1987) 111.
[42] W.J. Hehre, L. Radom, P.V.R. Schleyer, J.A. Pople, Ab Initio Molecular Orbital Theory, Wiley, New York, 1986.
[43] M. Zahedi-Tabrizi, F. Tayyari, Z. Moosavi-Tekyeh, A. Jalali, S.F. Tayyari, Spectrochim. Acta. A 65 (2006) 387.
[44] A.P. Scott, L. Radom, J. Phys. Chem. 100 (1996) 16502.
[45] J. Spanget-Larsen, Chem. Phys. 240 (1999) 51.
[46] J.A. Larssen, D. Cremer, J. Mol. Struct. 485–486 (1999) 385.
[47] S.F. Tayyari, M. Zahedi-Tabrizi, H. Rahemi, H.A. Mirshahi, J.S. Emampour, M. Rajabi, F. Milani-Nejad, J. Mol. Struct. (THEOCHEM) 730 (2005) 17.
[48] S.F. Tayyari, M. Zahedi-Tabrizi, F. Tayyari, F. Milani-Nejad, J. Mol. Struct. (THEOCHEM) 637 (2003) 171–181.
[49] S.F. Tayyari, H. Raissi, F. Milani-Nejad, I.S. Butler, Vibrational Spectroscopy 26 (2001) 187–199.